An improved variable forgetting factor recursive least square-double extend Kalman filtering based on global mean particle swarm optimization algorithm for collaborative state of energy and state of health estimation of lithium-ion batteries.

LONG, T., WANG, S., CAO, W., ZHOU, H. and FERNANDEZ, C.

2023

An improved Variable Forgetting Factor Recursive Least Square-Double Extend Kalman Filtering based on global mean particle swarm optimization algorithm for collaborative state of energy and state of health estimation of lithium-ion batteries

Tao Long[a,b], Shunli Wang[a*,b], Wen Cao[a], Heng Zhou[a,b] , Carlos Fernandez[c]

[a]*School of Information Engineering, Southwest University of Science and Technology, Mianyang 621010, China;*[b]*College of Electrical Engineering, Sichuan University, Chengdu 610065, China;*[c]*School of Pharmacy and Life Sciences, Robert Gordon University, Aberdeen AB10-7GJ, UK.*

Abstract: Accurate assessment of SOE and SOH is a critical issue in the battery management system. This paper proposes an improved variable forgetting factor recursive least square-double extend Kalman filtering algorithm based on global mean particle swarm optimization to obtain a stable and accurate SOE and SOH at different ageing levels and temperatures. Firstly, this paper establishes a framework for the parameter identification of variable forgetting factors recursive least squares algorithm based on the global mean particle swarm optimization. Then, proposing a global mean particle swarm optimization search mechanism centered on variable time double extended Kalman filtering. Finally, The proposed algorithm is validated on the hybrid pulse power characterization (HPPC) and Beijing bus dynamic stress test (BBDST) datasets. The experimental results show that the MAE and RMSE of the SOE results based on the HPPC condition are less than 0.0096 and 0.0153 at -5 °C and 15 °C. Similarly, the estimation results based on the BBDST condition are less than 0.0094 and 0.0102, respectively. The SOH estimation errors are less than 0.02. Therefore, the variable forgetting factor recursive least square-double extend Kalman filtering based on global mean particle swarm optimization algorithm can achieve accurate and stable SOE and SOH at different ageing levels and temperatures.

Key words: global mean particle swarm optimization; double extend Kalman filtering; collaborative estimation; state of health; state of energy

***Corresponding author**: Shunli Wang. Tel: +86-15884655563. E-mail address: wangshunli1985@qq.com.

1. Introduction

The development of human society is dependent on innovation, and the automotive industry is developing rapidly through innovation and transcendence [1, 2]. New energy vehicles (Nevs) have become a new trend in the development of the automotive industry, and the safety of Nevs is receiving more and more attention [3]. However, With the increasing popularity of Nevs, their charge/discharge problems are gradually increasing, which is very unfavorable for the development of Nevs [4, 5]. Therefore the evaluation of the state of energy (SOE) and state of health (SOH) of Lithium-ion batteries are gradually becoming an essential issue in battery management systems (BMS) and has attracted the attention of a large number of researchers

SOE is defined as the remaining available energy of the battery in real time, and an accurate estimation result of it will facilitate the stable and reliable operation of Nevs. Current national and international methods of estimating SOE include equivalent circuit model-based, data-driven, and hybrid methods. In the first place, Tian et al. and Tian et al. use the second-order RC equivalent circuit model to estimate state of charge (SOC) and SOH, respectively [6, 7]. To get a better result, Li et al. introduction of battery hysteresis voltage segmentation into a second-order RC model to form an improved second-order RC model, and the estimation results error is under 0.0431 [8]. Furthermore, for researching charging safety and SOC, Zhang et al. and Xu et al. use an improved back propagation (BP) neural network to get results [9, 10]. Liu et al. establish a lithium-ion battery internal short-circuit diagnosis model by combining a convolutional neural network [11], and the mean absolute error is under 1.8%. However, data-driven methods usually have time-consuming problems, requiring large amounts of data and poor generalization. Additionally, Wang et al., Hu et al., and Ma et al. introduce a hybrid method that combines the Extended Kalman filter (EKF) with back propagation (BP) neural network to get SOC, and the estimation error under 0.0141, 0.0240, and 0.0121, respectively [12-14]. However, the hybrid methods reduce some errors but increase the amount of computation. Consequently, the equivalent circuit model-based has attracted much attention due to its simplicity, reliability, and stability.

Current national and international methods based on equivalent circuit models usually include the Thevenin model, electrochemical model, and PNGV model. Previously, some researchers would estimate the SOE and state of power (SOP) of lithium-ion batteries using the first-order Thevenin equivalent circuit model [15, 16]. However, the first-order Thevenin model is difficult to achieve with the required precision. For instance, Zhang et al. introduce an application-oriented multistate estimation framework to estimate state values. However, the model parameters need optimization by EKF, particle swarm optimization, and recursive least square [17]. Li et al. and An et al. all use least squares to estimate the parameters but require compensation with an improved Kalman algorithm [18, 19]. Therefore, the other researchers used the second-order Thevenin model to estimate SOC and SOE. For example, Yang et al. and Zhang et al. estimate results error is less than 0.0193 and 0.02 based on the second-order Thevenin model, respectively [20, 21]. Zhang et al. introduce a novel non-experiment-based reconstruction method and use second-order Thevenin model as the basic structure and the mean absolute error can be limited under 0.01 [22]. Besides this, some electrochemical models have also been researched. Wu et al. and Liu et al. use a simplified electrochemical model to realize SOC estimation, and the mean absolute error is less than 0.02 and 0.0135 under constant and dynamic loading conditions, respectively [23, 24]. Zhang et al. introduce an equivalent circuit model and electrochemical impedance spectroscopy (EIS)-based technique to estimate SOC and SOH, and the estimation error can reach 1.29% [25]. However, electrochemical equipment is often expensive and prevents us from doing research.

SOE estimation based on equivalent circuit models requires accurate parameter identification results. Recursive least squares (RLS) and genetic algorithm (GA) are the more popular parameter identification methods. For example, Zhang et al. used an immune genetic algorithm to identify the model parameters and the error between voltage and reference voltage is less than 20 mV [26]. Zhang et al. used a particle swarm optimization (PSO) algorithm to improve accuracy of genetic algorithm [27]. Jiang et al. presented a random mutation ant colony optimization (RMACO) algorithm to parameter identification [28]. In this process, PSO

algorithm is found to be well optimized for parameter identification. However, GA is not very good at solving large scale computational problems and can easily fall into "precocious". Recursive least square is widely used in the parameter identification for lithium-ion batteries due to their simple implementation, computational simplicity, and stable performance. For instance, Li et al. added a variable forgetting factor to improve the robustness and accuracy of the traditional recursive least squares algorithm [29]. Shi et al. introduced a variable forgetting factor with the difference between open circuit and terminal voltages in sliding window mode based on recursive least square parameter identification approach. It can improve efficiency of data utilization [30]. Therefore, it can be seen that using an optimization algorithm to improve the accuracy of parameter identification is a better trend.

Once good parameter identification results have been obtained, selecting a suitable SOE estimation algorithm is core to the whole BMS. Due to the unique characteristics of the Kalman filter (KF), it has been developed and improved by many researchers and is used in many industries, such as aviation, marine and automotive. For example, Moradi et al. used Kalman filtering to analyze linear frequency modulated (FM) or chirp signal problems [31]. KF is used in real-time road target detection and tracking for autonomous driving to provide accurate pose and velocity information about objects moving on the road around the vehicle [32]. It can be seen that the KF is only suitable for use in linear systems. However, lithium-ion batteries are highly non-linear systems, and conventional Kalman filtering cannot be used directly for estimation. Therefore, some researchers have made many improvements to enable the Kalman filter to work on non-linear systems. For instance, Zhang et al. indicated an Extended Kalman filtering to estimate SOC, and the estimation error is within 1.10% [33]. Lee et al. estimated information feedback by using an extended Kalman filter to mitigate excessive battery operation [34]. Hou et al. introduced an adaptive unscented Kalman filtering (AUKF) algorithm to estimate SOE, and the proposed algorithm can adaptively correct the SOE values [35]. Shrivastava et al. used a double extended Kalman filtering (DEKF) to estimate the different battery states concurrently, the estimation results

error is less than 0.01, and experimental results show that DEKF algorithm has excellent multi-parameter estimation characteristics [36]. Besides this, Shrivastava et al. also proposed a new dual forgetting factor-based adaptive extended Kalman filter (DFFAEKF) algorithm. It is based on the DEKF algorithm and can estimate SOE and SOC [37]. Thus, it can be seen that adaptive joint estimation is the focus of researchers' attention.

In practice, the service life of lithium-ion batteries is shortened with the reduction of state of health (SOH). Many researchers currently estimate SOH including data-driven and feature-based methods. For example, Zhang et al. used a temporal convolutional network to fit relationship between SOH and temperature variety rate and SOH predicted values are less than 0.0145 [38]. Feng et al. presented a novel SOH estimation model based on relevance vector machine (RVM) [39]. Zhang et al. introduced an improved Particle Swarm Optimization Extreme Learning Machine for estimating SOH and remaining useful life (RUL). The results show that SOH estimation error is 0.033 [40]. Zhu et al. used a linear regression model to estimate SOH and the experimental results show a linear relationship between charging time and state of health with an error of less than 0.012 [41]. However, the lack of data support will affect the accuracy of SOH estimation, which is a difficult aspect of SOH estimation. Therefore, feature-based methods are more widely used in state of health prediction. For instance, Peng et al. developed a capacity degradation model based on the KF algorithm, and the results show that strain can be used as an indicator for estimating state of health [42]. Zhu et al. used an improved unscented particle filter algorithm to estimate SOH [43]. Adaptive algorithms have also been applied to SOH estimation. Jiang et al. proposed a comprehensive co-estimation scheme of SOC and SOH based on an adaptive extended Kalman filter (AEKF), The estimated capacity and internal resistance are less than 0.017 and 0.022, respectively [44]. Qian et al. introduced a modified-sine-cosine algorithm based on DEKF. A modified-sine-cosine algorithm improves the covariance noise matrix in the state filter. The experiment results show that proposed algorithm can reduce errors and correct initial values [45].

To fully explore the performance of intelligent optimization and model-based algorithms. This paper proposes

a novel double extended Kalman filtering collaborative state of energy and state of health estimation algorithm based on the global mean particle swarm optimization (GLPSO) algorithm. The main contributions of this paper are as follows.

(1) Variable forgetting factors recursive least squares can improve the accuracy of the model parameters identification through changing the forgetting factor in real time.

(2) The improved DEKF algorithm is used to estimate the SOE and update the model parameters online to obtain state of health. In addition, estimation time can set a controlled time step to reduce it.

(3) The GLPSO algorithm is introduced to solve the manual adjusting parameters problem, which significantly reduces the proposed algorithm estimation error and adjustment time.

2. Mathematical analysis

2.1 Improved variable forgetting factors recursive least squares

Recursive least squares (RLS) is a common mathematical optimization technique to obtain parameter estimation results for a system that minimizes the sum of squares of the errors between the observed data and estimation values. The algorithm is simple in principle, easy to implement, and widely used for online identification of lithium-ion battery model parameters. However, RLS algorithm still has drawbacks compared with genetic algorithms or particle swarm optimization. For example, with increasing recursions, the new data becomes difficult to correct and the algorithm loses its tracking and correction ability, which in turn affects the parameter estimation. Therefore, this paper introduces an improved variable forgetting factor to correct estimation errors.

Compared with the conventional forgetting factor recursive least squares (FFRLS) algorithm, improved variable forgetting factor recursive least squares (VFFRLS) can actively change the size of the forgetting factor according to the error value in real-time, rather than being limited to a single number, thus solving the problem

of variable data in complex operating conditions. The main process can be described as

$$e(k) = E(k) - X(k)\hat{\theta}(k-1) \tag{1}$$

$$K(k) = \frac{P(k-1)\hat{\theta}(k)}{X^T(k)P(k-1)X(k) + \lambda(k-1)} \tag{2}$$

$$\hat{\theta}(k) = \hat{\theta}^-(k) + K(k)e(k) \tag{3}$$

$$P(k) = \frac{(I - K(k)X^T(k))P(k-1)}{\lambda(k-1)} \tag{4}$$

$$\lambda(k) = \lambda_{min} + (1 - \lambda_{min})h^{\sigma(k)} \tag{5}$$

$$\sigma(k) = rou(\frac{e(k)}{e_{ba}}) \tag{6}$$

Where $X(k)$ is including current and voltage, $E(k)$ indicates the errors between estimating voltage and real voltage, $\hat{\theta}(k)$ indicates the results of the estimated model parameters, $K(k)$ indicates the Kalman gain, $P(k)$ is the covariance matrix, e_{ba} is usually taken with the expected error, *h* takes values ranging from 0 to 1, which indicates the sensitivity of the forgetting factor for error variation, *rou* indicates taking the nearest number, λ_{min} usually sets 0.98 according to RLS part of the introduction, $\lambda(k)$ indicates a dynamically changing forgetting factor, it can dynamically adjust the size of the forgetting factor according to the estimation errors between the terminal and simulated voltage in real-time.

According to equation (5) and equation (6), it can be seen that when system simulated voltage changes obviously, such as, the prediction $e(k)$ increases and $\sigma(k)$ increases quickly. However, $\lambda(k)$ will decrease rapidly since *h* is between 0 and 1, then prediction state values will forget the previous data and fit the new data quickly. In turn, with the boosting input of fresh values, the fitting data gradually converged, the prediction $e(k)$ decreases and $\sigma(k)$ decreases quickly, accordingly, $\lambda(k)$ will increase rapidly, so that the retained valid data ensures the algorithm to have high accuracy and strong robustness.

Considering equivalent circuit model can more accurately simulate the dynamic performance of the lithium-ion batteries. Therefore, the second-order Thevenin is chosen as the object of parameter identification and state estimate, as shown in Fig.1. This model consists of voltage sources U_b, an ohmic resistor R_i, and two

RC electric networks including polarization resistors (R_1 and R_2) and polarization resistors capacitance (C_1 and C_2), which can reflect the phenomenon of gradual voltage changes after charging and discharging and the end of the process.

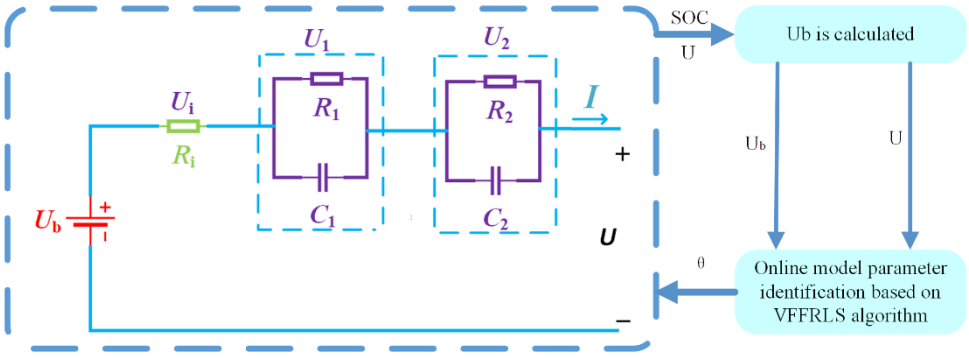

Fig. 1 Second order Thevenin model and parametric identification framework.

In Fig. 1, to complete the process of identifying the variable forgetting factor recursive least squares parameters based on the second order Thevenin model, it is necessary to calculate the model to obtain the required characteristic equations. According to Kirchhoff's laws, the model can be described as

$$\begin{cases} \mathrm{U} = U_b - U_1 - U_2 - I(t)R_i \\ \dfrac{dU_1}{dt} = -\dfrac{U_1}{R_1C_1} + \dfrac{I}{C_1} \\ \dfrac{dU_2}{dt} = -\dfrac{U_2}{R_2C_2} + \dfrac{I}{C_2} \end{cases} \tag{7}$$

According to Eq.(7), which can be obtained the Laplace transform expression of second order Thevenin model and present calculated process of variable forgetting factor recursive least squares. The equation process can be described as

$$\mathrm{U}_b = \left(\frac{R_1}{R_1C_1s+1} + \frac{R_2}{R_2C_2s+1} + R_i\right)\mathrm{I}+U \tag{8}$$

In the Eq.(8), s is the Laplacian operator. Define $E_L(s) = U(s) - U_b(s)$, which can be obtained the transfer function of continuous time system. So the model equation can be rewritten as

$$G(s) = \frac{E_L(s)}{I_L(s)} = -(R_i + \frac{R_1}{R_1C_1s+1} + \frac{R_2}{R_2C_2s+1}) \tag{9}$$

Using the bilinear transformation, the transfer function of the discrete-time system can calculate by Eq.(9) rewritten as

$$G(z^{-1}) = \frac{\theta_3 + \theta_4 z^{-1} + \theta_5 z^{-2}}{1 - \theta_1 z^{-1} + \theta_2 z^{-2}} \tag{10}$$

Define $\hat{\theta}(k) = [\theta_1, \theta_2, \theta_3, \theta_4, \theta_5]$, θ_n will be used as the basic parameter for parameter R_1, C_1, R_2, C_2, R_i, which can be described as

$$\begin{cases} R_i = \dfrac{\theta_3 - \theta_4 + \theta_5}{1 + \theta_1 - \theta_2} \\ R_1 C_1 R_2 C_2 = \dfrac{T^2(1 + \theta_1 - \theta_2)}{4(1 + \theta_1 - \theta_2)} \\ R_1 C_1 + R_2 C_2 = \dfrac{T(1 - \theta_2)}{4(1 + \theta_1 - \theta_2)} \\ R_i + R_1 + R_2 = \dfrac{\theta_3 + \theta_4 + \theta_5}{1 - \theta_1 - \theta_2} \\ R_i R_1 C_1 + R_i R_2 C_2 + R_1 R_2 C_1 + R_1 R_2 C_2 = \dfrac{T(\theta_5 - \theta_3)}{4(1 - \theta_1 - \theta_2)} \end{cases} \tag{11}$$

In the Eq.(11), the T is a simple time. Define the Coefficient matrix of the system $X(k) = [E_L(k-1), E_L(k-1), -I(k), -I(k-1), -I(k-2)]$ for preparing parameter process. Suppose a, b, c, d, and f are used as coefficients in Eq.(11), so the expression can be rewritten as

$$\begin{cases} a = \dfrac{\theta_3 - \theta_4 + \theta_5}{1 + \theta_1 - \theta_2} \\ \mathrm{b} = \dfrac{T^2(1 + \theta_1 - \theta_2)}{4(1 + \theta_1 - \theta_2)} \\ \mathrm{c} = \dfrac{T(1 - \theta_2)}{4(1 + \theta_1 - \theta_2)} \\ \mathrm{d} = \dfrac{\theta_3 + \theta_4 + \theta_5}{1 - \theta_1 - \theta_2} \\ \mathrm{f} = \dfrac{T(\theta_5 - \theta_3)}{4(1 - \theta_1 - \theta_2)} \end{cases} \tag{12}$$

Define $\tau_1 = (c + \frac{\sqrt{c^2 - 4b}}{2})$, $\tau_2 = (c - \frac{\sqrt{c^2 - 4b}}{2})$. Thus , the R_1, C_1, R_2, C_2, R_i can be obtained by recursive algorithm. Combined with Eq. (12) and Eq. (11), the parameter results can be rewritten as

$$\begin{cases} R_i = a \\ R_1 = |d - a - R_2| \\ R_2 = \dfrac{d - a \times \tau_2 - d \times \tau_1}{\tau_2 - \tau_1} \\ C_1 = \dfrac{\tau_2}{R_1} \\ C_2 = \dfrac{\tau_1}{R_2} \end{cases} \tag{13}$$

After the above analysis, a reasonable initial value of $X(k)$ and $\hat{\theta}(k)$ can be obtained. Setting $P_0 = 1$, the

values of $K(k)$ can be obtained according to Eq.(2). Therefore, reasonable initial values allow the VFFRLS algorithm starts fitting iteratively over time to obtain model parameter values in real time.

2.2 Variable time double extended Kalman filter

To accomplish the joint state of energy and state of health estimation of lithium-ion batteries is necessary to estimate state and parameter variables simultaneously, so a double extended Kalman filter (DEKF) algorithm for collaborative estimation parameters is used in this paper. However, traditional double extended Kalman filtering can only be used to estimate SOC and SOH and cannot handle the collaborative SOE and SOH estimation and the division of the estimated time domain. Therefore, this paper introduces a novel variable time double extended Kalman filter to collaborative SOE and SOH estimation in real-time, the model state space equation can be described as

$$\begin{cases} x_{k+1} = f(x_k, u_k, \theta_k) + w_k \\ y_k = h(x_k, u_k, \theta_k) + v_k \end{cases} \tag{14}$$

In the Eq. (14), w_k and v_k indicate Gaussian noise in the state equation and output equation, respectively. θ_k represents system parameter vector, which can achieve state and parameter estimation time division. So the system parameter calculation of algorithm can be rewritten as

$$\begin{cases} \theta_{k+1} = \theta_k + o_k \\ l_k = g(x_k, u_k, \theta_k) + e_k \end{cases} \tag{15}$$

In the Eq. (15), o_k represents the parameter slowly changing process and e_k represents observation noise. So the different time variation domains can be obtained by adjusting o_k. The variable time double extended Kalman filter structure can be divided into four parts, including determining the state transfer matrix, parameter initiation, time update, and state update.

First step, the state transition matrix of the system can be described as

$$\begin{cases} A_{k-1} = \dfrac{\partial f(x_k, u_k, \theta_k^-)}{\partial x_{k-1}} \\ C_k^x = \dfrac{\partial f(x_k, u_k, \theta_k^-)}{\partial x_{k-1}} \\ C_k^\theta = \dfrac{\partial g(x_k^-, u_k, \theta_k)}{\partial \theta} \end{cases} \tag{16}$$

In the Eq. (16), x_k^- is the prior estimate of the state variable at time *k*, C_k^x and C_k^θ are for the system state and system parameters respectively. x_0 θ_0 P_{x_0} P_{θ_0}

The second step, initialize the algorithm parameters, the process can be described as

$$x_0 = E(x_0), P_{x_0} = E[(x_0 - \widehat{x_0})(x_0 - \widehat{x_0})^T] \tag{17}$$

$$\theta_0 = E(\theta_0), P_{\theta_0} = E[(\theta_0 - \widehat{\theta_0})(\theta_0 - \widehat{\theta_0})^T] \tag{18}$$

$$P_w = E[ww^T], P_v = E[vv^T], P_o = E[oo^T], P_w = E[ee^T] \tag{19}$$

P_{θ_0} is the covariance matrix of the system parameter. P_{x_0} is the covariance matrix of the system state. $\widehat{x_0}$ and $\widehat{\theta_0}$ are represented estimation values. E indicates the expected value.

Third step, time update for x and θ. P_w and P_o indicate the covariance matrix of the corresponding parameter. which can be described as

$$P_{\theta_k}^- = P_{\theta_{k-1}} + P_o \tag{20}$$

$$P_{x_k}^- = A_{k-1} P_{x_{k-1}} A_{k-1}^T + P_w \tag{21}$$

Fourth step, state update for *x* and θ, which can be described as

$$\begin{cases} K_k^\theta = P_{\theta_k}^- \left(C_k^\theta\right)^T \left(C_k^\theta P_{\theta_k}^- \left(C_k^\theta\right)^T + P_e\right)^{-1} \\ \theta_k = \theta_k^- + K_k^\theta [y_k - g(x_k^-, u_k, \theta_k^-)] \\ P_{\theta_k} = (I - K_k^\theta C_k^\theta) P_{\theta_k}^- \end{cases} \tag{22}$$

$$\begin{cases} K_k^x = P_{x_k}^- (C_k^x)^T \left(C_k^x P_{x_k}^- (C_k^x)^T + P_v\right)^{-1} \\ x_k = x_k^- + K_k^x [y_k - g(x_k^-, u_k, \theta_k^-)] \\ P_{x_k} = (I - K_k^x C_k^x) P_{x_k}^- \end{cases} \tag{23}$$

In the Eq.(22) and Eq.(23), the superscripts θ and *x* are divided into corresponding system parameter and state values, K indicates Kalman gain, C_k^θ and C_k^x represent the state transfer matrix of the system parameter and state, I represents unit matrix, P_e and P_v indicate measure noise covariance for state filter and parameter

filter respectively. The equation show that one of the extended Kalman filter performs the parameter estimation, the other performs the system state and then the final result is the collaborative SOE and SOH estimation. The flow chart of the variable time DEKF algorithm, as shown in Fig. 2.

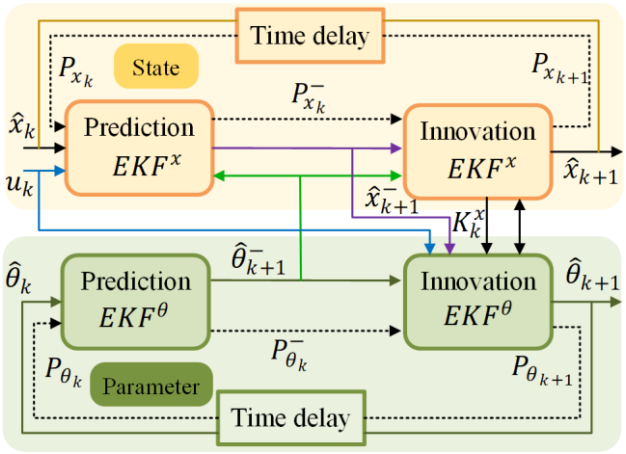

Fig. 2 the flow chart of Variable time double extended Kalman filter

In Fig. 2, the top extended Kalman filter outputs the SOE parameter, x_k, and the bottom filter outputs the model parameters, θ_k. The required parameters are obtained by setting different time delays between State and Parameter filters and iterating the 4-step calculation. According to Fig.1, Discrete the circuit model to obtain the state equations and output equations. The state equation for the system state variable of the first EKF can be described as

$$\begin{bmatrix} SOE(k) \\ U_1 \\ U_2 \end{bmatrix} = \begin{bmatrix} e^{\left(-\frac{T}{R_1C_1}\right)} & 0 & 0 \\ 0 & e^{\left(-\frac{T}{R_2C_2}\right)} & 0 \\ 0 & 0 & 1 \end{bmatrix} \begin{bmatrix} SOE(k-1) \\ U_1(k-1) \\ U_2(k-1) \end{bmatrix} + \begin{bmatrix} R_1\left(1-e^{-\frac{T}{R_1C_1}}\right) \\ R_2\left(1-e^{-\frac{T}{R_2C_2}}\right) \\ -\frac{Tu_k}{3600E} \end{bmatrix} I(\mathrm{k}+1) + Q_1 \tag{24}$$

The output equation can be described as

$$U^x(k) = U_b[SOE(k)] - U_1(k) - U_2(k) - R_iI(k) + R_1 \tag{25}$$

In the Eq. (24), $A_k = \begin{bmatrix} e^{\left(-\frac{T}{R_1C_1}\right)} & 0 & 0 \\ 0 & e^{\left(-\frac{T}{R_2C_2}\right)} & 0 \\ 0 & 0 & 1 \end{bmatrix}$, $B_k = \begin{bmatrix} R_1\left(1-e^{-\frac{T}{R_1C_1}}\right) \\ R_2\left(1-e^{-\frac{T}{R_2C_2}}\right) \\ -\frac{Tu_k}{3600E} \end{bmatrix}$, $C_k^x = [\frac{\partial U^x(k)}{\partial SOE(k)} - 1 - 1]$. The state equation for the system parameter variable of the second EKF can be described as

$$\begin{bmatrix} R_1(k) \\ R_2(k) \\ C_1(k) \\ C_2(k) \\ R_i(k) \\ Q_m(k) \end{bmatrix} = \begin{bmatrix} R_1(k-1) \\ R_2(k-1) \\ C_1(k-1) \\ C_2(k-1) \\ R_i(k-1) \\ Q_m(k-1) \end{bmatrix} + Q_2 \tag{26}$$

The output equation can be described as

$$U^{\theta}(k) = U_b[SOE(k)] - U_1(k) - U_2(k) - R_i I(k) + R_2 \tag{27}$$

In the Eq, Q_1, Q_2, R_1, and R_2 are the error covariance matrices for w, o, v and e respectively. The discretized state and output equations are brought into the variable time DEKF algorithm to update the SOE values and the current maximum capacity of the lithium-ion batteries in real time. Besides this, using the remaining charge definition method to define the battery SOH and equation can be described as

$$SOH = \frac{Q_m}{Q_f} \times 100\% \tag{28}$$

In the Eq. (28), Q_f indicates the rated capacity of the battery, Q_m indicates the estimated maximum available capacity. The algorithm can be realized with the above algorithm formula for collaborative SOE and SOH estimation of lithium-ion batteries.

2.3 Global mean particle swarm optimization algorithm

The particle swarm optimization algorithm simulates a bird in a flock by designing a massless particle with only two properties: velocity (v_i), which represents the speed of movement, and position (x_i), which represents the direction of movement. Each particle searches for the optimal solution in the search space, which is recorded as the current individual extreme value (I_{ev}), and shares the extreme individual value with the other particles in the whole particle swarm. I_{ev} is used as the current global optimal solution for the whole swarm, and other particles will adjust their velocity and position according to compare with global I_{ev} and their own I_{ev}.

In each iteration, the particle updates estimation parameters by tracking two "extreme values" (p_{best}, g_{best}), p_{best} indicates the individual optimal values, g_{best} indicates the group optimal values. Once found, the

particle updates the velocity and position using the following formula, which can be described as

$$v_i = w \times v_i + c1 \times rand() \times (p_{best} - x_i) + c2 \times rand() \times (g_{best} - x_i) \tag{29}$$

$$x_i = x_i + v_i \tag{30}$$

In the Eq. (28), i indicates the number of particles, $c1$ and $c2$ indicate learning factor, $rand()$ indicates a random number between 0 and 1, w indicates inertia factor, which normally has a negative value and calculates can be described as

$$w = w_{max} - ((w_{max} - w_{min}) \times \frac{\text{ger} - \text{itern}}{\text{ger}}) \tag{31}$$

In the Eq. (31), $w_{max} = 0.9$, $w_{min} = 0.4$, ger indicates the number of cycles, itern the current number of cycles. The introduction of linearly decreasing weight (LDW) can make a significant improvement to the PSO algorithm. However, considering the limitations of the traditional PSO algorithm, the instability of the VFFRLS parameter estimation and the inadequacy of experiential tuning of the parameters in the DEKF algorithm. This paper introduces a global mean particle swarm optimization algorithm to optimize the above parameters together. The algorithm structure, as shown in Fig. 3.

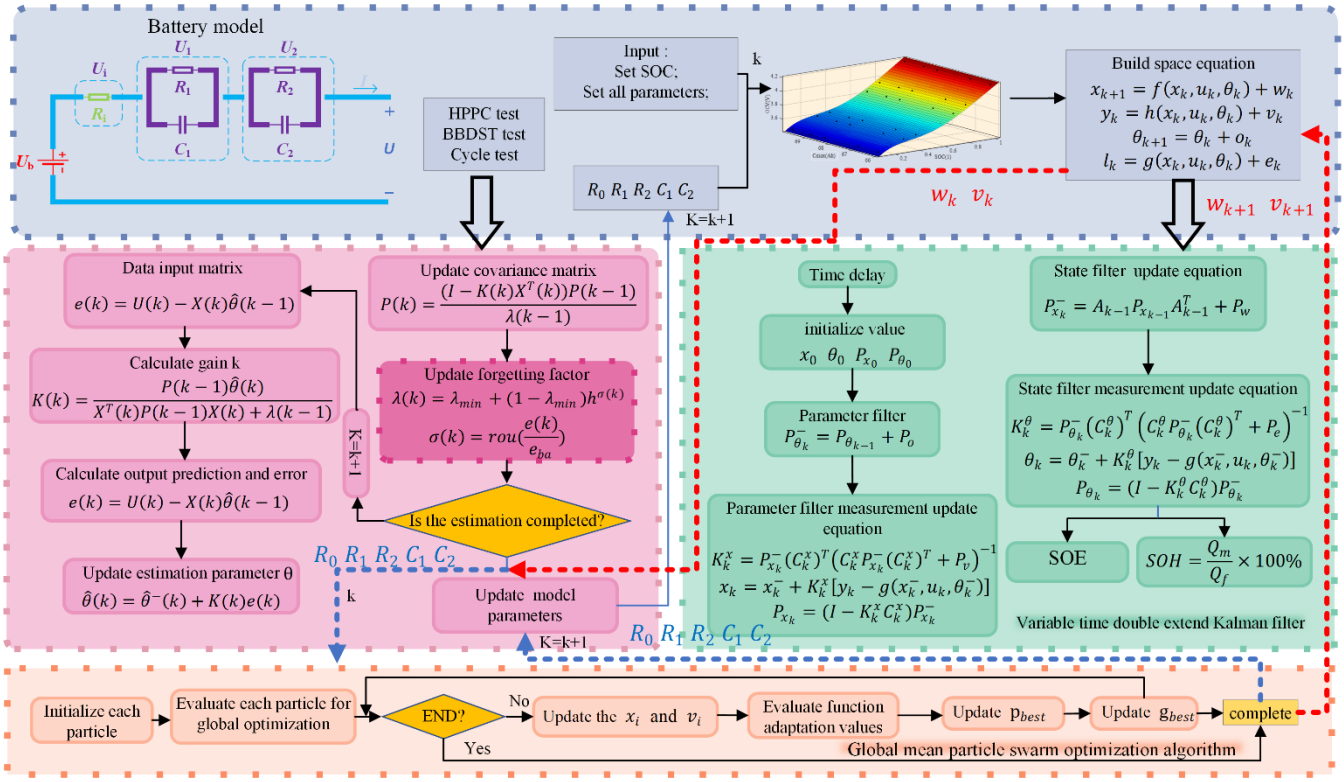

Fig. 3 the flow chart of VFFRLS-DEKF based on global mean particle swarm optimization algorithm

As shown in Fig. 3, the whole algorithm is divided into four parts, including battery model, VFFRLS algorithm, variable time DEKF algorithm and global mean particle swarm optimization (GLPSO). Since we cannot directly observe the process signal and measure the noise covariance, the value of P_w and P_e are obtained by searching for GLPSO. Besides this, the VFFRLS online parameter identification results are mean-sorted by the GLPSO algorithm to obtain the optimal R_i, R_1, R_2, C_1, and C_2 results, respectively. Addresses the errors caused by fluctuating online parameter identification results, manual parameter adjustment, and improves the accuracy of its estimation.

3. Experimental analysis

This paper takes a 70 Ah ternary lithium-ion battery as the research object and builds an independent test battery test platform, including BMS-HIL-1005 Model and max power is 1500 W, it performs data acquisition. HT-HW-80 thermostat with a temperature range of -40 to +150 (℃). The Charging and discharging equipment is CT-4016-5V100A-NTFA and the power is 12 Kw, which can realize hybrid pulse power characterization (HPPC) and Beijing bus dynamic stress test (BBDST). The experimental team has already carried out a series of battery

testing experiments on this platform (https://www.researchgate.net/project/Whole-Life-Cycle-Test). The lithium-ion batteries test platform, as shown in Fig. 4.

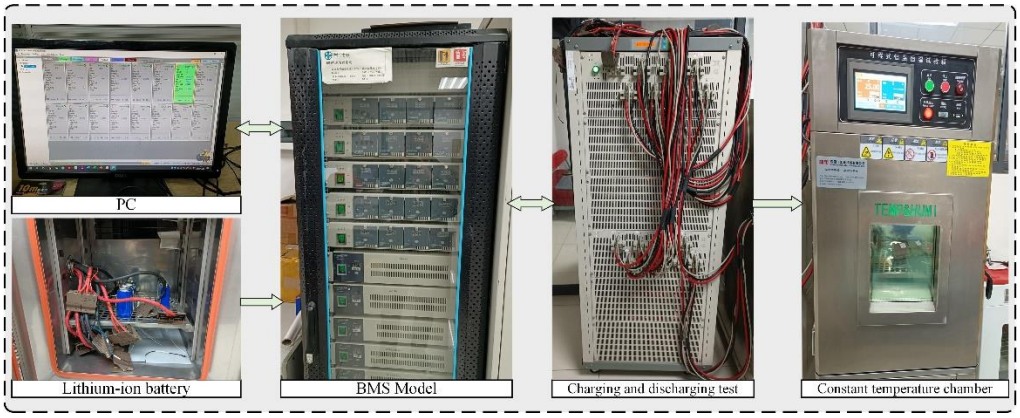

Fig. 4 Lithium-ion batteries test platform

This paper uses lithium-ion batteries test platform to obtain HPPC and BBDST experimental data at -5 and 15 degrees. The working condition voltage and current test results, as shown in Fig. 5.

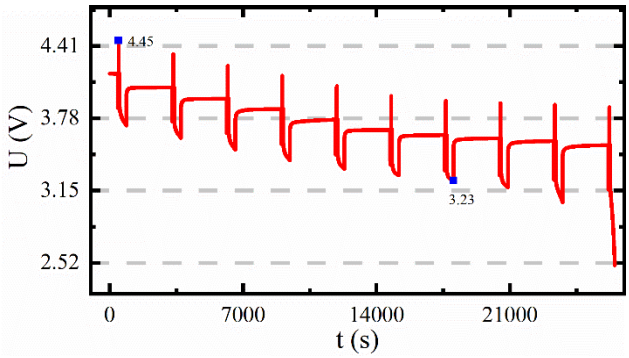

(a) voltage of HPPC test under -5 ℃

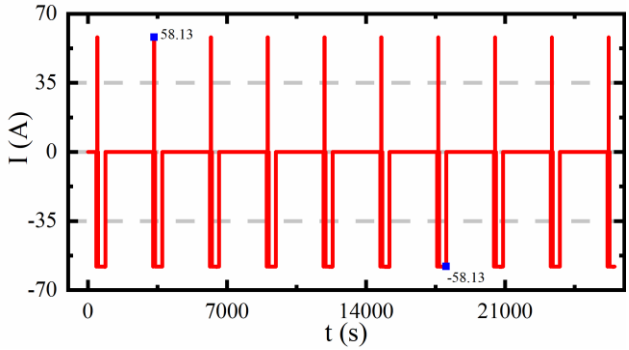

(b) current of HPPC test under -5 ℃

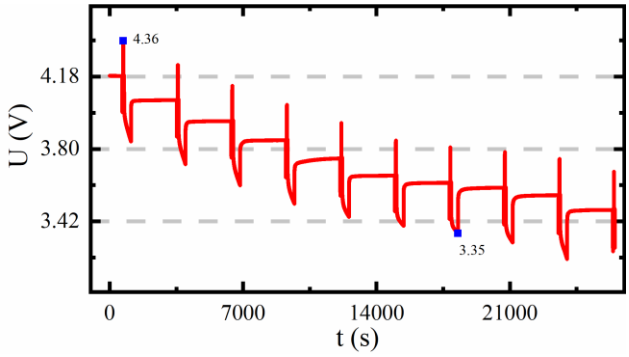

(c) voltage of HPPC test under 15 ℃

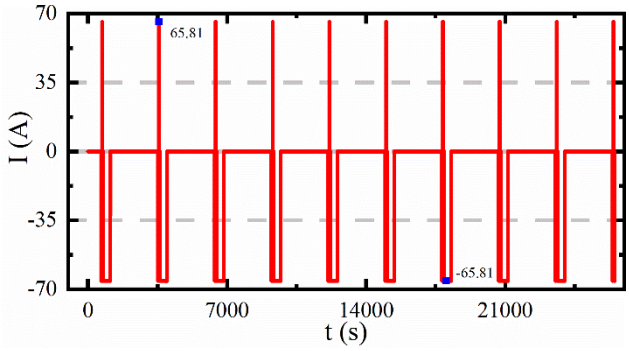

(d) current of HPPC test under 15 ℃

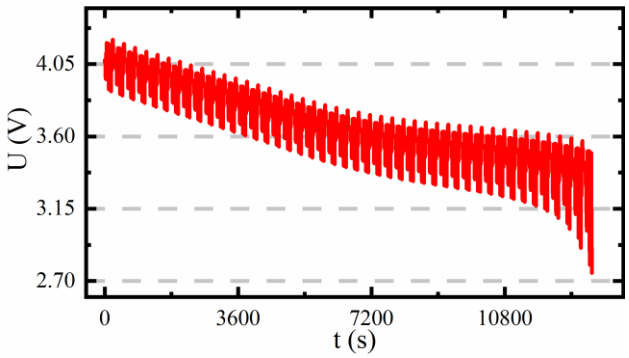

(e) voltage of BBDST test under -5 ℃

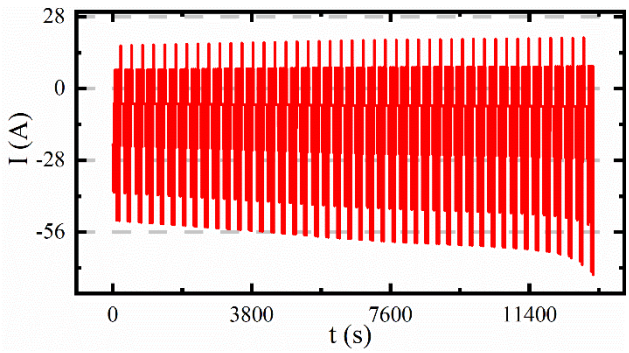

(f) current of BBDST test under -5 ℃

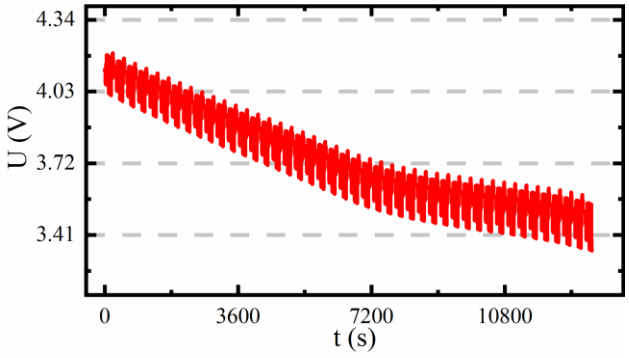

(g) voltage of BBDST test under 15 ℃

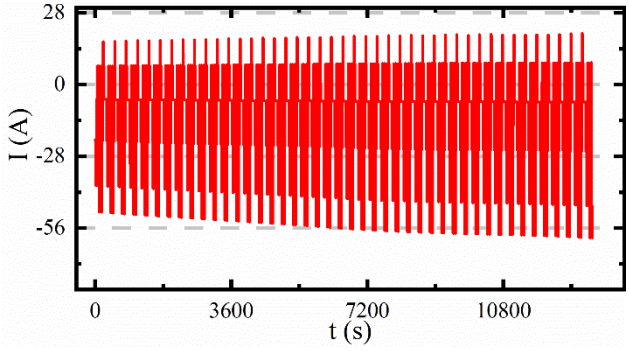

(h) current of BBDST test under 15 ℃

Fig. 5 HPPC and BBDST test current and voltage results

3.1 Global mean value parameter identification results

Using HPPC test at -5 degrees to verify the accuracy of the proposed GLPSO-VFFRLS algorithm parameter identification. Firstly, VFFRLS algorithm is used online to identify $R_1, C_1, R_2, C_2,$ and R_i of the second-order Thevenin model online, respectively. Then, to verify that offline parameter identification is better than online, a multi-objective GLPSO algorithm is used to optimize the parameter results. The estimation results, as shown in Fig. 6.

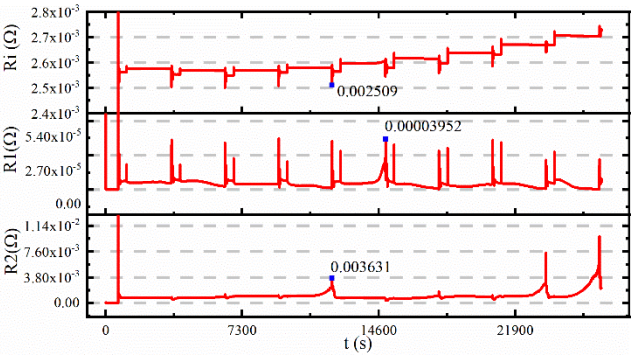

(a) Resistance identification results

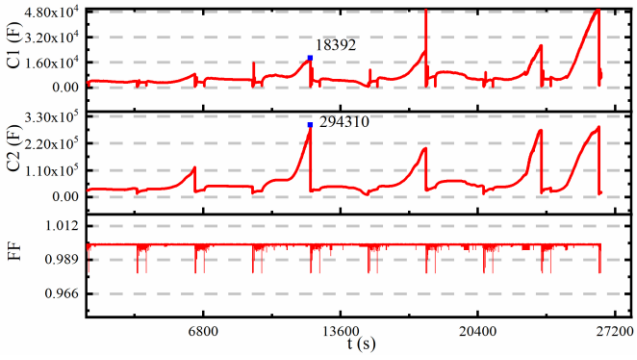

(b) Capacitance identification results and forgetting

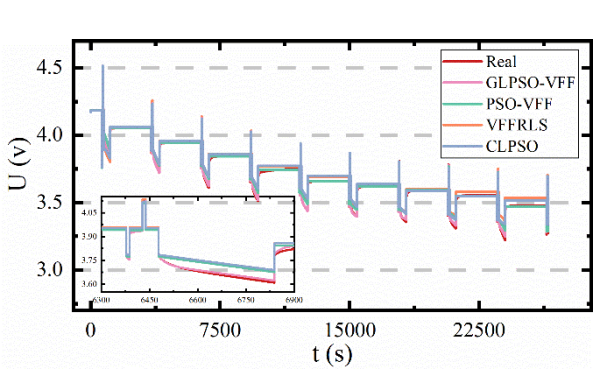

(c) Analogue voltage comparison results

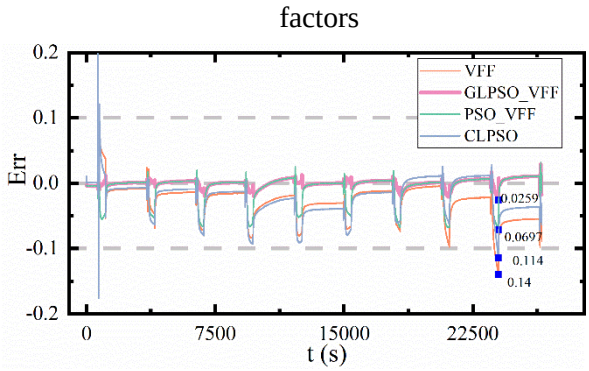

(d) Analog voltage error comparison results

Fig. 6 Parameter identification and simulated voltage results of the algorithm

As shown in Fig.6 (a) and (b), the $R_1, C_1, R_2, C_2,$ and R_i online identification results and the variation of the forgetting factor are shown respectively. (b) shows that the forgetting factor varies simultaneously with the variation of the parameters, ranging from 0.99 to 0.94. However, there are large fluctuations in the simulated voltage errors after bringing the online identification results into the second-order Thevenin model. For example, VFFRLS and Comprehensive Learning particle swarm optimization (CLPSO) online identification algorithms achieve a maximum simulated voltage error and Mean Absolute Error (MAE) of 0.14 V, 0.114 V, and 0.028, 0.025, respectively. Therefore, using GLPSO to perform an average global search for the optimal identification results of the VFFRLS algorithm, the maximum simulated voltage error and MAE of GLPSO-VFFRLS algorithm are 0.03 V and 0.0042, respectively. Besides this, the PSO-VFFRLS algorithm simulates voltage errors and MAE is 0.0697 V and 0.01101. The results show that GLPSO-VFFRLS is significantly better than the other algorithms and meets the accuracy requirements.

3.2 collaborative estimation results of SOE and SOH

HPPC and BBDST working conditions at -5 °C and 15 °C were used to estimate SOE and SOH and verify the accuracy of the proposed algorithm in this section. Besides this, the PSO-DEKF, DEKF and long short term memory (LSTM) algorithm are used as comparative experiments with proposed algorithm. The SOE and SOH estimate results, as shown in Fig. 7, Fig. 8, and Fig. 9.

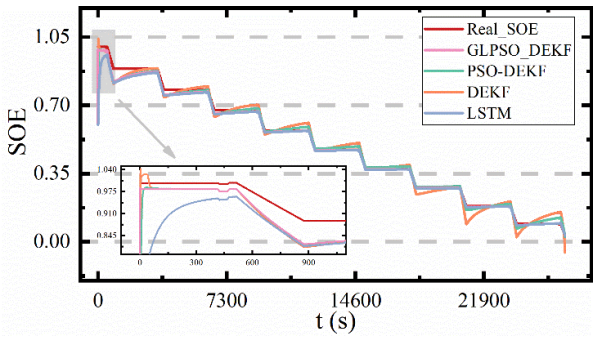

(a) SOE estimation results at -5 °C

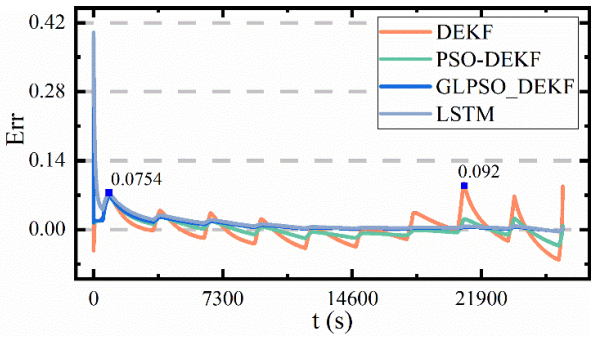

(b) SOE estimation error at -5 °C

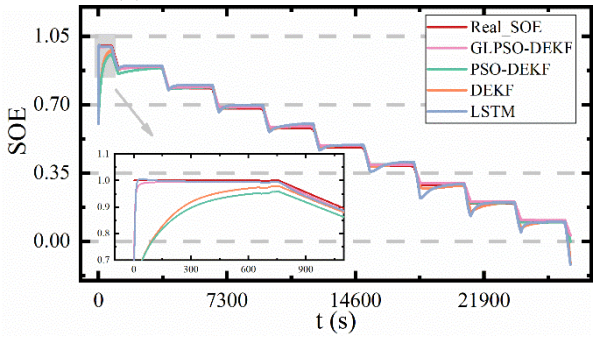

(c) SOE estimation results at 15 °C

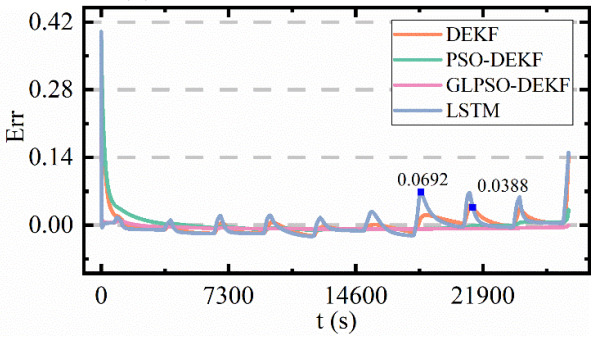

(d) SOE estimation error at 15 °C

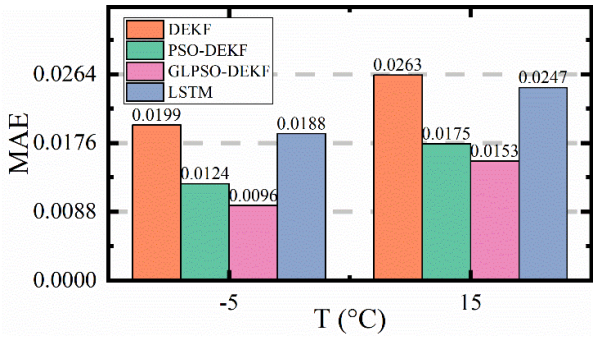

(e) Comparison results of four algorithms MAE

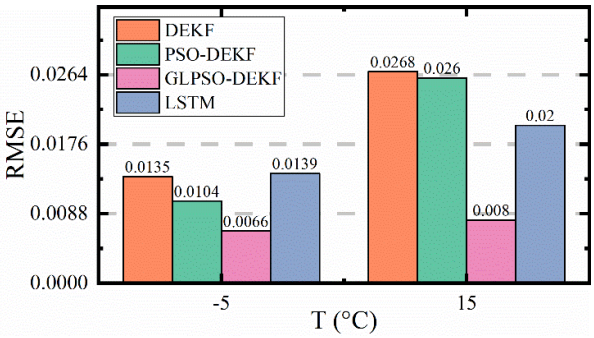

(f) Comparison results of four algorithms RMSE

Fig. 7 SOE estimation results under HPPC working conditions

As shown in Fig. 7, the state of energy estimation curve based on the DEKF algorithm has large fluctuates, and the phenomenon is particularly obvious with the SOE gradually decreasing. Especially at 15 °C, the PSO-DEKF and LSTM algorithms estimate the SOE curve with an increasingly significant fluctuation error, which cannot meet the daily requirements. From this, it can be seen that single-objective optimization only leads to improvements in individual parameters and cannot achieve the required accuracy. LSTM often shows large fluctuations at low state of energy due to underfitting and overfitting problems. In contrast, at ambient temperatures of -5 °C and 15 °C, the proposed GLPSO-DEKF algorithm can effectively reduce error fluctuations and converge quickly. In particular, the algorithm is more robust at low state of energy. The MAE

and RMSE of the four algorithms as shown in Fig. 7 (e) and (f). According to (e) and (f), the MAE and RMSE of the GLPSO-DEKF algorithm outperformed the other algorithms at all temperatures. For example, at 15 degrees, the maximum error and RMSE are below 0.01. Thus, the algorithm has better accuracy in the HPPC condition. The algorithms estimate results under the BBDST condition, as shown in Fig. 8.

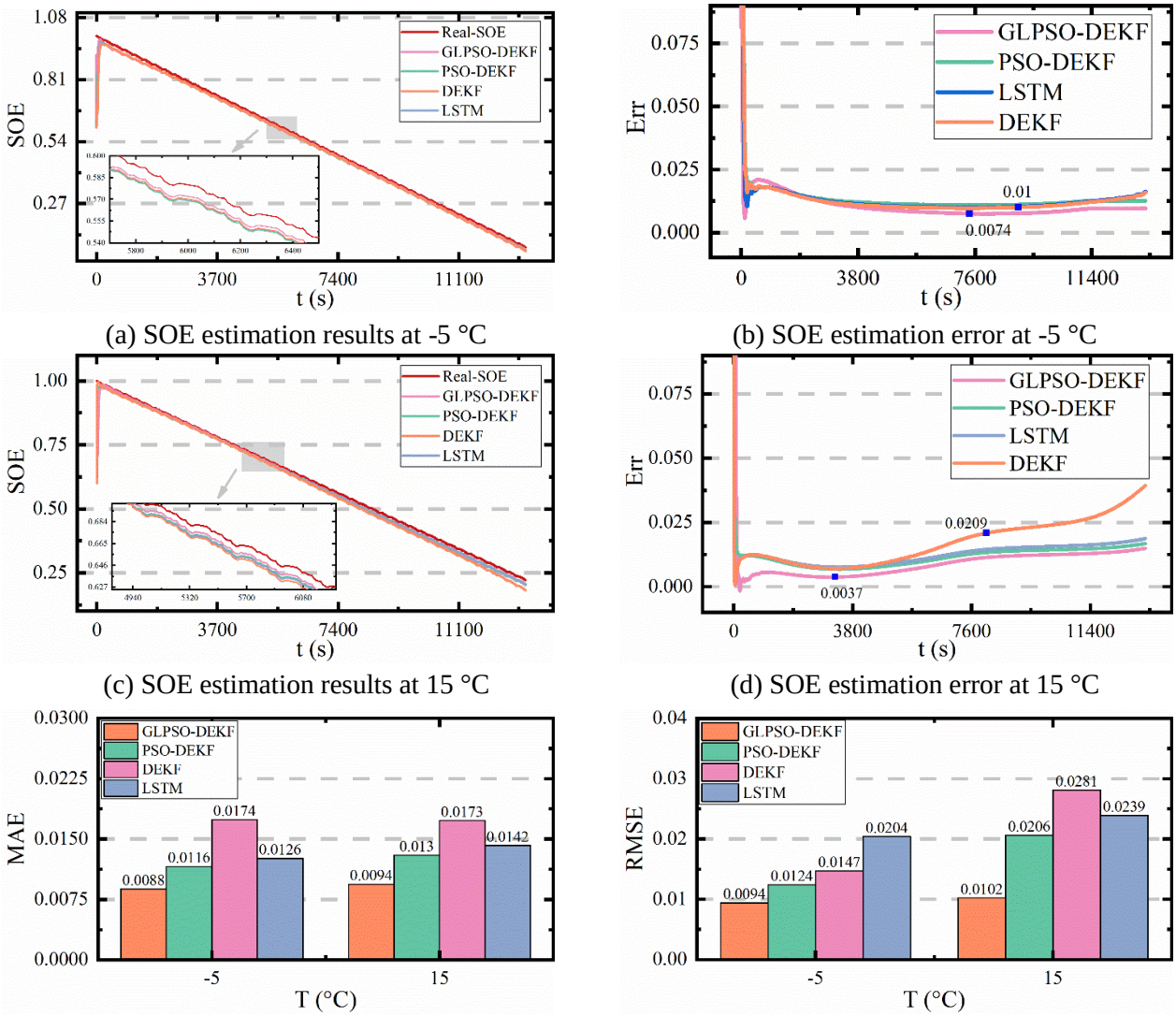

(a) SOE estimation results at -5 °C

(b) SOE estimation error at -5 °C

(c) SOE estimation results at 15 °C

(d) SOE estimation error at 15 °C

(e) Comparison results of four algorithms MAE

(f) Comparison results of four algorithms RMSE

Fig. 8 SOE estimation results under BBDST working conditions

As shown in Fig. 8, the four algorithms show low error fluctuations at -5 °C. However, the GLPSO-DEKF algorithm achieves a minimum error of 0.0074 and the DEKF algorithm only reaches 0.01. The proposed algorithm is significantly better than the other algorithms. At an ambient temperature of 15 °C, the DEKF algorithm exhibits large error fluctuations and cannot obtain a stable SOE estimate. However, the proposed

GLPSO-DEKF algorithm achieves an accurate accuracy of 0.0037 and converges consistently. Similarly, according to fig. (e) and (f), the values of MAE and RMSE for the four algorithms are presented. It can be seen that the DEKF algorithm is 0.0174 and GLPSO-DEKF algorithm is 0.0088, with the DEKF being twice as large as the GLPSO-DEKF algorithm. Besides this, the value of GLPSO-DEKF is 0.5 times smaller than PSO-DEKF and LSTM, which again reflects the instability of single-objective optimization and underfitting problem under BBDST working conditions. At the same time, this further demonstrates that the proposed GLPSO-DEKF algorithm is beneficial in reducing the state of energy estimation error and improving the adaptability and robustness. This paper uses the real capacity of lithium-ion batteries with different levels of ageing as reference values and performs SOH experiments at temperatures of -5 °C and 15°C under the HPPC and BBDST conditions, respectively, as shown in Fig. 9.

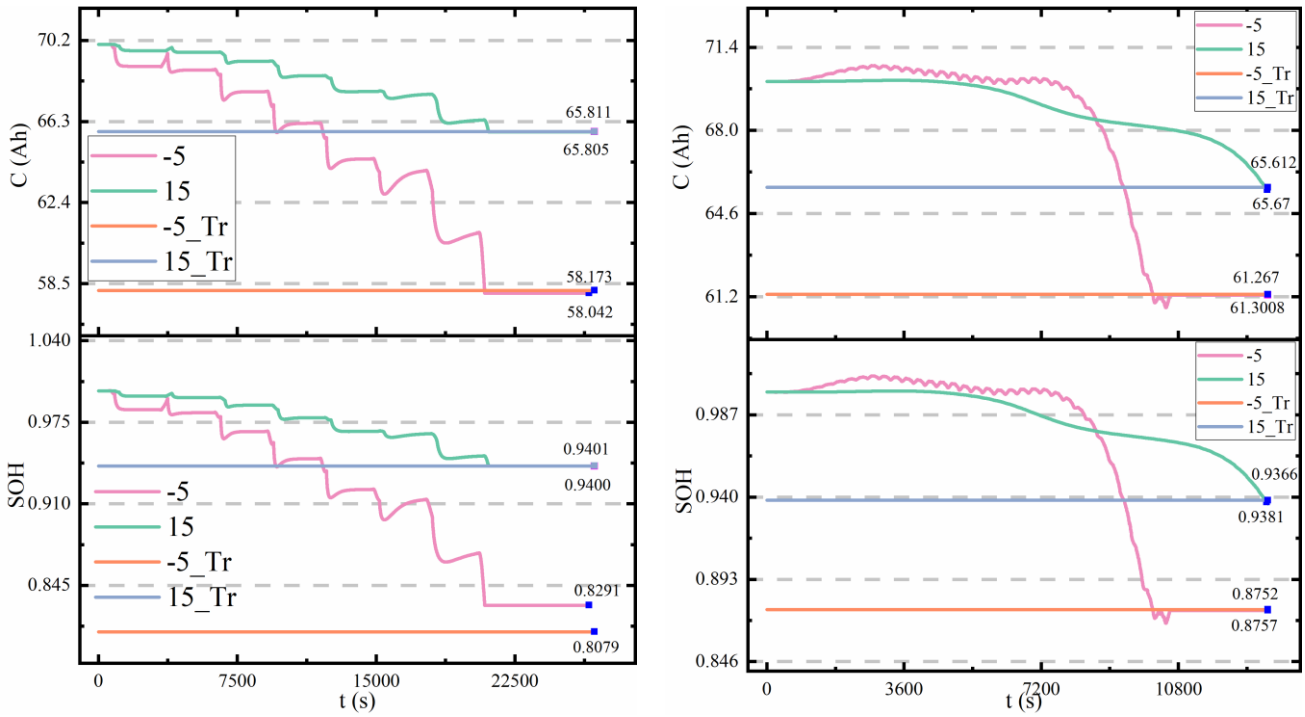

(a) SOH estimation results under HPPC test (b) SOH estimation results under BBDST test

Fig. 9 SOH estimation results for different aging levels and temperatures

According to Fig. 9 (a), it can be seen that the algorithm can accurately estimate the true capacity under HPPC and BBDST conditions. For example, the capacity estimation errors are 0.006 Ah and 0.0131 Ah at 15 °C and

-5°C, respectively. Similarly, the capacity estimation errors are 0.062 Ah and 0.0338 Ah under BBDST conditions. Besides this, the SOH estimation errors are below 0.02 for both HPPC and BBDST conditions. Therefore, the proposed GLPSO-DEKF algorithm can effectively improve the estimation accuracy of state of health.

4. Conclusions

This paper proposed an improved variable forgetting factor recursive least square-double extend Kalman filtering based on GLPSO algorithm for collaborative state of energy and state of health estimation of lithium-ion batteries. Firstly, the VFFRLS algorithm can actively change the size of the forgetting factor according to the error value in real time. Then, the VFFRLS-DEKF algorithm does not need manual adjustment parameters. Specifically, when the VFFRLS-DEKF algorithm is in the iterative process, the global mean particle swarm optimization will automatically find the optimal parameters to improve the accuracy of the SOE and SOH. In addition, the proposed algorithm is evaluated under different operating conditions at different temperatures separately, including HPPC and BBDST conditions at -5 ℃ and 15℃. The experiment results show that the proposed algorithm can accurately collaborate SOE and SOH estimation. The MAE and RMSE values of SOE are less than 0.016 and 0.011 under two conditions, respectively. Meanwhile, the SOH estimation errors are less than 0.02 at different aging degrees. However, the algorithm will have large fluctuations and lead to poor results when the battery is at low capacity. In future work, we will try to combine algorithms with neural networks to adapt to wide temperature environments and different levels of aging batteries.

Acknowledgments

The work was supported by National Natural Science Foundation of China (No. 62173281).

References

[1]. Zhang, L., et al., *Globalization, Green Economy and Environmental Challenges: State of the Art Review for Practical Implications.* Frontiers in Environmental Science, 2022. **10**.

[2]. Fernando, Y., et al., *Eco-innovation impacts on recycled product performance and competitiveness: Malaysian automotive industry.* Sustainable Production and Consumption, 2021. **28**: p. 1677-1686.

[3]. Tan, Z., et al., *Charging Behavior Analysis of New Energy Vehicles.* Sustainability, 2021. **13**(9).

[4]. Tarhan, B., O. Yetik, and T.H. Karakoc, *Hybrid battery management system design for electric aircraft.* Energy, 2021. **234**.

[5]. Xie, K., et al., *A method for measuring and evaluating the fault response performance of battery management system.* Energy Reports, 2022. **8**: p. 639-649.

[6]. Tian, Y., et al., *State of charge estimation of lithium-ion batteries based on cubature Kalman filters with different matrix decomposition strategies.* Energy, 2022. **238**.

[7]. Tan, X., et al., *Online state-of-health estimation of lithium-ion battery based on dynamic parameter identification at multi timescale and support vector regression.* Journal of Power Sources, 2021. **484**.

[8]. Li, J., et al., *Equivalent Circuit Modeling and Parameter Identification for Lithium-ion Batteries Based on Improved Barnacle Mating Optimizer.* Sensors and Materials, 2022. **34**(9): p. 3649-3670.

[9]. Zhang, L., et al., *Research on electric vehicle charging safety warning model based on back propagation neural network optimized by improved gray wolf algorithm.* Journal of Energy Storage, 2022. **49**.

[10]. Xu, H., et al., *A novel Drosophila-back propagation method for the lithium-ion battery state of charge estimation adaptive to complex working conditions.* International Journal of Energy Research, 2022. **46**(11): p. 15864-15880.

[11]. Liu, Y., et al., *Internal Short Circuit Diagnosis of Lithium-Ion Battery Based on Mechanism Model and Deep Learning.* Journal of the Electrochemical Society, 2022. **169**(10).

[12]. Ma, Q.Y., et al., *The state of charge estimation of lithium-ions battery using combined multi-population genetic algorithm-BP and Kalman filter methods.* International Journal of Electrochemical Science, 2022. **17**(2).

[13]. Wang, C., et al., *A Novel BCRLS-BP-EKF Method for the State of Charge Estimation of Lithium-ion Batteries.* International Journal of Electrochemical Science, 2022. **17**(4).

[14]. Hu, Y.F., et al., *Joint Dynamic Strategy of Bayesian Regularized Back Propagation Neural Network with Strong Robustness - Extended Kalman Filtering for the Battery State-of-Charge Prediction.* International Journal of Electrochemical Science, 2021. **16**(11).

[15]. Lai, X., et al., *A novel method for state of energy estimation of lithium-ion batteries using particle filter and extended Kalman filter.* Journal of Energy Storage, 2021. **43**.

[16]. Guo, R. and W. Shen, *An enhanced multi-constraint state of power estimation algorithm for lithium-ion batteries in electric vehicles.* Journal of Energy Storage, 2022. **50**.

[17]. Zhang, S., N. Peng, and X. Zhang, *An application-oriented multistate estimation framework of lithium-ion battery used in electric vehicles.* International Journal of Energy Research, 2021.

[18]. Li, X.Y., et al., *State of energy estimation for a series-connected lithium-ion battery pack based on an adaptive weighted strategy.* Energy, 2021. **214**.

[19]. An, F., et al., *State of Energy Estimation for Lithium-Ion Battery Pack via Prediction in Electric Vehicle Applications.* Ieee Transactions on Vehicular Technology, 2022. **71**(1): p. 184-195.

[20]. Yang, X., et al., *A novel fuzzy adaptive cubature Kalman filtering method for the state of charge and state of energy co-estimation of lithium-ion batteries.* Electrochimica Acta, 2022. **415**.

[21]. Zhang, S. and X. Zhang, *A novel low-complexity state-of-energy estimation method for series-connected lithium-ion battery pack based on "representative cell" selection and operating mode division.* Journal of Power

Sources, 2022. **518**.

[22]. Zhang, S. and X. Zhang, *A novel non-experiment-based reconstruction method for the relationship between open-circuit-voltage and state-of-charge/state-of-energy of lithium-ion battery.* Electrochimica Acta, 2022. **403**.

[23]. Liu, L., J. Zhu, and L. Zheng, *An Effective Method for Estimating State of Charge of Lithium-Ion Batteries Based on an Electrochemical Model and Nernst Equation.* Ieee Access, 2020. **8**: p. 211738-211749.

[24]. Wu, L., et al., *Online SOC Estimation Based on Simplified Electrochemical Model for Lithium-Ion Batteries Considering Current Bias.* Energies, 2021. **14**(17).

[25]. Zhang, Q., et al., *Electrochemical Impedance Spectroscopy Based State-of-Health Estimation for Lithium-Ion Battery Considering Temperature and State-of-Charge Effect.* Ieee Transactions on Transportation Electrification, 2022. **8**(4): p. 4633-4645.

[26]. Zhengxin, J., et al., *An Immune Genetic Extended Kalman Particle Filter approach on state of charge estimation for lithium-ion battery.* Energy, 2021. **230**.

[27]. Zhang, L., et al., *A fractional-order model of lithium-ion batteries and multi-domain parameter identification method.* Journal of Energy Storage, 2022. **50**.

[28]. Jiang, Z.Y., et al., *Fractional modeling and parameter identification of lithium-ion battery.* Ionics, 2022. **28**(9): p. 4135-4148.

[29]. Li, M., et al., *A Battery SOC Estimation Method Based on AFFRLS-EKF.* Sensors, 2021. **21**(17).

[30]. Shi, J., H. Guo, and D. Chen, *Parameter identification method for lithium-ion batteries based on recursive least square with sliding window difference forgetting factor.* Journal of Energy Storage, 2021. **44**.

[31]. Moradi, E. and R. Mohseni, *Parameters estimation of linear frequency modulated signal using Kalman filter and its extended versions.* Signal Image and Video Processing, 2022.

[32]. Farag, W., *Kalman-filter-based sensor fusion applied to road-objects detection and tracking for autonomous vehicles.* Proceedings of the Institution of Mechanical Engineers Part I-Journal of Systems and Control Engineering, 2021. **235**(7): p. 1125-1138.

[33]. Zhang, Y., et al., *Novel Feedback-Bayesian BP Neural Network Combined with Extended Kalman Filtering for the Battery State-of-Charge Estimation.* International Journal of Electrochemical Science, 2021. **16**(6).

[34]. Lee, T.-K. and Z.S. Filipi, *Nonlinear lithium-ion diffusion dynamics conscious power management strategy in hybrid electric vehicles for battery downsizing.* Proceedings of the Institution of Mechanical Engineers Part D-Journal of Automobile Engineering, 2012. **226**(D7): p. 857-868.

[35]. Hou, E., et al., *Research on State of Power Estimation of Echelon-Use Battery Based on Adaptive Unscented Kalman Filter.* Symmetry-Basel, 2022. **14**(5).

[36]. Shrivastava, P., et al., *Model-based state of X estimation of lithium-ion battery for electric vehicle applications.* International Journal of Energy Research, 2022. **46**(8): p. 10704-10723.

[37]. Shrivastava, P., et al., *Combined State of Charge and State of Energy Estimation of Lithium-Ion Battery Using Dual Forgetting Factor-Based Adaptive Extended Kalman Filter for Electric Vehicle Applications.* Ieee Transactions on Vehicular Technology, 2021. **70**(2): p. 1200-1215.

[38]. Zhang, D., et al., *Evaluation of the State of Health of Lithium-Ion Battery Based on the Temporal Convolution Network.* Frontiers in Energy Research, 2022. **10**.

[39]. Feng, H. and H. Yan, *State of health estimation of large-cycle lithium-ion batteries based on error compensation of autoregressive model.* Journal of Energy Storage, 2022. **52**.

[40]. Zhang, C.-y., et al., *Improved Particle Swarm Optimization-Extreme Learning Machine Modeling Strategies for the Accurate Lithium-ion Battery State of Health Estimation and High-adaptability Remaining Useful Life Prediction.* Journal of the Electrochemical Society, 2022. **169**(8).

[41]. Zhu, X., et al., *State of health estimation of lithium-ion battery by removing model redundancy through aging mechanism.* Journal of Energy Storage, 2022. **52**.

[42]. Peng, J., et al., *State estimation of lithium-ion batteries based on strain parameter monitored by fiber Bragg*

grating sensors. Journal of Energy Storage, 2022. **52**.

[43]. Zhu, F. and J. Fu, *A Novel State-of-Health Estimation for Lithium-Ion Battery via Unscented Kalman Filter and Improved Unscented Particle Filter.* Ieee Sensors Journal, 2021. **21**(22): p. 25449-25456.

[44]. Jiang, N. and H. Pang, *Study on Co-Estimation of SoC and SoH for Second-Use Lithium-Ion Power Batteries.* Electronics, 2022. **11**(11).

[45]. Qian, K.F. and X.T. Liu, *Hybrid optimization strategy for lithium-ion battery's State of Charge/Health using joint of dual Kalman filter and Modified Sine-cosine Algorithm.* Journal of Energy Storage, 2021. **44**.